POLITECNICO DI TORINO
Repository ISTITUZIONALE

A GNSS Multipath and NLoS Mitigation Method for Urban Scenarios Based on Particle Filtering

Original
A GNSS Multipath and NLoS Mitigation Method for Urban Scenarios Based on Particle Filtering / Zocca, Simone; Guo, Yihan; Dovis, Fabio. - ELETTRONICO. - (2024), pp. 575-588. (Intervento presentato al convegno 2024 International Technical Meeting of The Institute of Navigation tenutosi a Long Beach, California (USA) nel January 23 - 25, 2024) [10.33012/2024.19565].

Availability:
This version is available at: 11583/2987008 since: 2024-03-14T17:16:28Z

Publisher:
The Institute of Navigation

Published
DOI:10.33012/2024.19565

Terms of use:

This article is made available under terms and conditions as specified in the corresponding bibliographic description in the repository

Publisher copyright
GENERICO -- per es. Nature : semplice rinvio dal preprint/submitted, o postprint/AAM [ex default]

The original publication is available at https://doi.org/10.33012/2024.19565 / http://dx.doi.org/10.33012/2024.19565.

(Article begins on next page)

28 April 2024

A GNSS Multipath and NLoS Mitigation Method for Urban Scenarios Based on Particle Filtering

Simone Zocca, Yihan Guo, Fabio Dovis, *Politecnico di Torino, Turin, Italy*

BIOGRAPHY

Simone Zocca received a B.Sc. in Telecommunication Engineering in 2018 and a M.Sc. in Communication and Computer Networks Engineering in 2020, both from Politecnico di Torino (Turin, Italy). He is currently a Ph.D. student within the Navigation Signal Analysis and Simulation - NavSAS - group at the Department of Electronics and Telecommunications (DET) of Politecnico di Torino. His research is focused on innovative solutions for signal processing techniques and Bayesian estimation applied to Global Navigation Satellite System (GNSS)).

Yihan Guo received the B.Sc. degree from Northwestern Polytechnical University (Xi'an, Shaanxi, China) in 2016, and the M.Sc. degree from Shanghai Jiao Tong University (Shanghai, China) in 2019. He is a Ph.D. student at the Department of Electronics and Telecommunications (DET) of Politecnico di Torino (Turin, Italy) and a member of the Navigation Signal Analysis and Simulation - NavSAS - group. His current research interests include integrated navigation systems based on Global Navigation Satellite System (GNSS) and Ultra-Wideband (UWB).

Fabio Dovis received the M.Sc. and Ph.D. degrees from the Politecnico di Torino, Turin, Italy, in 1996 and 2000, respectively. In 2004, he joined the Department of Electronics and Telecommunications, where he has been a Full Professor since 2021. He coordinates the Navigation, Signal Analysis and Simulation Research Group (NavSAS). His research addresses the design of Global Navigation Satellite System (GNSS) receivers, and advanced signal processing for GNSS impairments. He authored more than 70 journal papers and more than 150 papers in conference proceedings. He is a member of the IEEE Aerospace and Electronic Systems Society (AESS) navigation systems panel, and he is currently serving on the Council of the US Institute of Navigation (ION). He is a member of the GNSS Scientific Advisory Committee (GSAC) of the European Space Agency (ESA).

ABSTRACT

Global navigation satellite systems (GNSSs) are at the basis of many location services. However, in harsh environments such as urban canyons, the performance can be highly degraded due to lack of satellite visibility and complex reflection phenomena like multipath and Non-Line-of-Sight (NLoS). This work aims at exploiting the consistency of the information provided by GNSS receivers to detect and mitigate the effect of multipath and NLoS on the positioning solution. The proposed method extends the definition of innovation for the Particle Filter (PF), while also exploiting its native capability to handle more complex probability models of the errors. The use of multi-modal probability densities adds robustness to the filter in harsh conditions. The proposed method has been tested on real open-source datasets, showing considerable improvement in terms of position error compared to other state-of-the-art solutions based on the Extended Kalman Filter (EKF).

I. INTRODUCTION

In recent years, Global Navigation Satellite System (GNSS) has become ubiquitous for providing localisation information to emerging technologies, such as autonomous vehicles, precision agriculture, smart wearables, etc EUSPA (2022). However, its standalone performance may be degraded in harsh scenarios such as urban canyons, thus limiting its usage capabilities Zhu et al. (2018b). The main source of GNSS faults in urban scenario are multipath and Non-Line-of-Sight (NLoS) Chen et al. (2013); Groves and Jiang (2013); Joerger and Pervan (2016); Vilà-Valls et al. (2020). According to McGraw et al. (2020), multipath occurs when the receiver receives a signal via more than one path. On the other hand, NLoS reception happens when the signal is received through reflection, but only from a single path. Many different methodologies have been proposed to detect and mitigate the impact of multipath/NLoS. Most research can be categorised based on the stage of the receiver in which they are applied Strode and Groves (2016):

1. **Antenna-based techniques**: Multipath/NLoS are caused by the reflected signals, which have different polarisation and reception angles w.r.t. direct signals. Due to this, choke rings, dual-polarisation, and array antennas are some of the most popular solutions developed Taghdisi et al. (2021); Groves et al. (2010); Vagle et al. (2016).
2. **Receiver-based techniques**: For multipath, reflected signals cause a distortion of the auto-correlation in the code tracking loop in the signal processing stage. Therefore, more sophisticated tracking loops designs, such as narrow correlators, double-delta correlators, strobe correlators, and vector tracking, are exploited to detect and separate the reflected signals

McGraw and Braasch (1999); Sun et al. (2022); Wang and Huang (2020); Xu et al. (2019).

3. **Navigation-processor-based techniques**: Multipath/NLoS can result in inconsistencies between measurements in the positioning unit, including pseudorange, carrier phase, pseudorange rate, and signal strength. Some methods use measurement redundancy Chang et al. (2022) to perform statistical tests such as chi-square test to detect faults. Besides, 3D city maps and elevations and azimuths of satellites can be utilised as additional information to detect and mitigate faults Hsu (2017); Groves and Jiang (2013); Medina et al. (2018).

Regardless of the wide range of signal blockage and reflection scenarios that may occur, the effect is most often a bias introduced in the measurements. This research focuses on navigation-processor-based techniques because they have the possibility to detect and mitigate faults from most causes. In particular, it utilises the Particle Filter (PF) (whose advantages will be discussed in a later section) to detect and mitigate both multipath and NLoS. The PF has garnered increased attention in recent years for addressing the multipath/NLoS problem due to its robustness features. Previous work has systematically explored its potential within the Receiver Autonomous Integrity Monitoring (RAIM) framework Mohanty et al. (2021); Gupta and Gao (2019). In contrast to prior studies, this work primarily leverages information from the previous epoch provided by the particle filter to estimate pseudorange biases caused by multipath/NLoS, thereby mitigating their impact.

A main principle for detecting multipath/NLoS is to exploit redundancy, which allows the finding of faulty measurements producing large residuals. The redundancy can be split into two domains: the space domain and the time domain. The first refers to the possibility of observing multiple satellites in a single epoch, checking whether all the measurements match the solution under a certain error bound. One example is to check the consistency of measurements from different satellites Blanch et al. (2012) or using additional sensors like Inertial Navigation System (INS) to check its consistency with GNSS measurements Wang et al. (2020). On the other hand, time domain consistency is considered between two consecutive epochs Zhu et al. (2018a). The estimated states should change smoothly according to the motion of the user. Filtering-based approaches monitor the consistency over time using innovations of the filter Zhu et al. (2018a). The main reason for leveraging filtering techniques is to exploit additional redundancy from the time domain when satellite visibility is poor, and hence, redundancy in the space domain is limited. The contributions of this research can be detailed as:

1. The concept of innovation to determine multiple multipath/NLoS is extended to the PF.
2. A threshold of the PF innovation is derived, to detect multipath/NLoS for pseudorange measurements.
3. To mitigate the impact of multipath/NLoS, the measurement likelihood functions used in the PF are refined by modelling the multipath/NLoS term.

II. METHOD AND ALGORITHM

This section first shows the state-space formulation of GNSS Position, Velocity and Time (PVT) Spilker Jr et al. (1996). Then, the basic framework of the particle filter is introduced Särkkä (2013). The proposed multipath/NLoS detection and mitigation method is developed based on this framework.

1. GNSS state-space model

The state-space model for a filtering problem can be written in the form:

$$\boldsymbol{x}_k = \boldsymbol{f}\left(\boldsymbol{x}_{k-1}\right) + \boldsymbol{q}_{k-1} \tag{1}$$

$$\boldsymbol{y}_k = \boldsymbol{h}\left(\boldsymbol{x}_k\right) + \boldsymbol{r}_k \tag{2}$$

where $\boldsymbol{x}_k$ is a vector of states at epoch k; $\boldsymbol{y}_k$ is a vector of measurements at epoch k; $\boldsymbol{f}(\cdot)$ is a set of state transition functions representing the dynamic model; $\boldsymbol{h}(\cdot)$ is a set of measurement functions; $\boldsymbol{q}_{k-1} \sim \mathcal{N}\left(0, \boldsymbol{Q}_{k-1}\right)$ and $\boldsymbol{r}_k \sim \mathcal{N}\left(0, \boldsymbol{R}_k\right)$ are Gaussian distributed process and measurement noises, with zero-mean and known covariance matrices $\boldsymbol{Q}_{k-1}$ and $\boldsymbol{R}_k$, respectively. More in detail, the state vector $\boldsymbol{x}_k$ is composed of the state variables of interest:

$$\boldsymbol{x}_k = \left[\, \boldsymbol{s}_k \quad \delta t_{u,k} \quad \boldsymbol{v}_k \quad \delta f_{u,k} \,\right]^T \tag{3}$$

where vector $\boldsymbol{s}_k = [s_{x,k} \quad s_{y,k} \quad s_{z,k}]$ is the position of the receiver at epoch k in a Cartesian reference frame; vector $\boldsymbol{v}_k = [v_{x,k} \quad v_{y,k} \quad v_{z,k}]$ is the velocity of the receiver at epoch k; $\delta t_{u,k}$ and $\delta f_{u,k}$ are respectively the clock bias and clock drift of the receiver expressed in meters and meters per second. On the other hand, the measurement vector is:

$$\boldsymbol{y}_k = \left[\, \boldsymbol{\rho}_k \quad \dot{\boldsymbol{\rho}}_k \,\right]^T \tag{4}$$

where $\boldsymbol{\rho}_k$ is an M by 1 vector of pseudorange measurements w.r.t. to M visible satellites; $\dot{\boldsymbol{\rho}}_k$ is an M by 1 vector of pseudorange rate (Doppler) measurements. The dynamic model $\boldsymbol{f}(\cdot)$ is a discrete-time formulation given by the state transition matrix $\boldsymbol{F}_k$:

$$\boldsymbol{F}_k = \begin{bmatrix} \boldsymbol{I}_{3\times3} & \boldsymbol{0}_{3\times1} & \boldsymbol{I}_{3\times3}\Delta t & \boldsymbol{0}_{3\times1} \\ \boldsymbol{0}_{1\times3} & 1 & \boldsymbol{0}_{1\times3} & \Delta t \\ \boldsymbol{0}_{3\times3} & \boldsymbol{0}_{3\times1} & \boldsymbol{I}_{3\times3} & \boldsymbol{0}_{3\times1} \\ \boldsymbol{0}_{1\times3} & \boldsymbol{0}_{1\times1} & \boldsymbol{0}_{1\times3} & 1 \end{bmatrix} \tag{5}$$

where Δt is the time elapsed between consecutive epochs (i.e., discretisation step); $\boldsymbol{I}_{3\times3}$ is a 3-by-3 identity matrix. The measurement model $\boldsymbol{h}(\cdot)$ consists of the measurement functions of pseudorange and pseudorange rate. First, the pseudorange equation w.r.t satellite i is given by:

$$\begin{aligned} \rho_k^{(i)} = & \underbrace{\sqrt{(s_{x,k}^{(i)} - s_{x,k})^2 + (s_{y,k}^{(i)} - s_{y,k})^2 + (s_{z,k}^{(i)} - s_{z,k})^2}}_{r_k^{(i)}} \\ & + \delta t_{u,k} - \delta t_k^{(i)} + I_k^{(i)} + T_k^{(i)} + F_{\rho,k}^{(i)} + \epsilon_{\rho,k}^{(i)} \end{aligned} \tag{6}$$

where $\rho_k^{(i)}$ is the pseudorange w.r.t. satellite i at epoch k; $r_k^{(i)}$ is the geometrical distance between satellite i and the receiver at epoch k; Vector $\boldsymbol{s}_k^{(i)} = \begin{bmatrix} s_{x,k}^{(i)} & s_{y,k}^{(i)} & s_{z,k}^{(i)} \end{bmatrix}$ is the position of satellite i at epoch k; $\delta t_k^{(i)}$ is the clock bias of satellite i at epoch k; $I_k^{(i)}$ is the ionosphere delay w.r.t. satellite i at epoch k; $T_k^{(i)}$ is the troposphere delay w.r.t. satellite i at epoch k; $F_{\rho,k}^{(i)}$ is the ranging bias w.r.t. satellite i due to GNSS multipath/NLoS at epoch k; $\epsilon_{\rho,k}^{(i)}$ is the receiver noise in the pseudorange measurement from satellite i at epoch k. Then, the pseudorange rate equation w.r.t satellite i is given by:

$$\overbrace{-\lambda f_{d,k}^{(i)}}^{\dot{\rho}_k^{(i)}} = \left(\boldsymbol{v}_k^{(i)} - \boldsymbol{v}_k\right) \cdot \boldsymbol{\Phi}_k^{(i)} + \delta f_{u,k} + \epsilon_{\dot{\rho},k}^{(i)} \tag{7}$$

where λ is the nominal carrier wavelength of the transmitted signal; $f_{d,k}^{(i)}$ is the Doppler measurement from satellite i at epoch k; $\boldsymbol{\Phi}_k^{(i)}$ is a unit vector pointing from receiver to satellite i at epoch k; $\boldsymbol{v}_k^{(i)} = \begin{bmatrix} v_{x,k}^{(i)} & v_{y,k}^{(i)} & v_{z,k}^{(i)} \end{bmatrix}$ is the velocity vector of satellite i at epoch k; $\delta f_{u,k}$ is the receiver clock drift; $\epsilon_{\dot{\rho},k}^{(i)}$ is the receiver noise on the pseudorange rate measurement from satellite i at epoch k.

In the PF, the process noise $\boldsymbol{Q}_{k-1}$ is used to model the uncertainty about the dynamics of the receiver between observation times. The dynamic model in a discrete form with infinite terms can be written as:

$$\begin{aligned} \boldsymbol{s}_k &= \boldsymbol{s}_{k-1} + \boldsymbol{v}_{k-1}\Delta t + \frac{1}{2}\boldsymbol{a}_{k-1}\Delta t^2 + ... \\ \boldsymbol{v}_k &= \boldsymbol{v}_{k-1} + \boldsymbol{a}_{k-1}\Delta t + ... \\ \delta t_{u,k} &= \delta t_{u,k-1} + \delta f_{u,k-1}\Delta t + \frac{1}{2}\delta a_{u,k-1}\Delta t^2 + ... \\ \delta f_{u,k} &= \delta f_{u,k-1} + \delta a_{u,k-1}\Delta t + ... \end{aligned} \tag{8}$$

To make this model computation feasible, it can be truncated before the terms related to $\boldsymbol{a}_{k-1}$ and $\delta a_{u,k-1}$. As a result, all the neglected terms containing Δt and higher order derivatives of $\boldsymbol{s}_{k-1}$ and $\delta t_{u,k}$ contribute to the process noise. The typical measurement frequency of GNSS for land vehicles is equal or larger than $1\,\mathrm{Hz}$ ($\Delta t < 1\,\mathrm{s}$). Therefore, higher powers of Δt approach small values and higher order terms are negligible. Once the maximum values of acceleration $\boldsymbol{a}_{max}$ and receiver drift rate $\delta a_{max,u}$ are obtained according to the application at hand, the process noise can be tuned to account for the unmodeled terms in the dynamic model (8). Based on the three-sigma rule of the normal distribution, this research sets the standard deviation as $1/3$ of the maximum unmodeled terms containing $\boldsymbol{a}_{k-1}$ and $\delta a_{u,k-1}$ in the dynamic model. Therefore, the diagonal covariance

matrix is written as:

$$\boldsymbol{Q}_{k-1} = diag \begin{bmatrix} \left(\left(\frac{1}{3}\frac{1}{2}\boldsymbol{a}_{max}\Delta t^2\right)^2\right)^T \\ \left(\left(\frac{1}{3}\boldsymbol{a}_{max}\Delta t\right)^2\right)^T \\ \left(\frac{1}{3}\frac{1}{2}\delta a_{max,u}\Delta t^2\right)^2 \\ \left(\frac{1}{3}\delta a_{max,u}\Delta t\right)^2 \end{bmatrix} \tag{9}$$

In order to obtain the measurement noise covariance matrix $\boldsymbol{R}_k$, this research exploits an elevation-based model to determine the measurement noise variances $\sigma^2_{\rho^{(i)}}$ and $\sigma^2_{\dot{\rho}^{(i)}}$ for each pseudorange and pseudorange rate, respectively Wang et al. (1998):

$$\sigma^2_{\rho^{(i)}} = a^2_\rho + \frac{b^2_\rho}{sin\theta^{(i)}} \tag{10}$$

$$\sigma^2_{\dot{\rho}^{(i)}} = a^2_{\dot{\rho}} + \frac{b^2_{\dot{\rho}}}{sin\theta^{(i)}} \tag{11}$$

where a_ρ, b_ρ, $a_{\dot{\rho}}$, and $b_{\dot{\rho}}$ are model parameters, which should be determined for every specific type of the GNSS module, $\theta^{(i)}$ is the elevation angle for satellite i.

2. Particle Filter

The PF, a member of the sequential Monte Carlo methods, aims to approximate the posterior Probability Density Function (PDF) of the state-space by employing Bayes' formula. In the context of nonlinear filtering problems, the goal is to compute the PDF $p(\boldsymbol{x}_k|\boldsymbol{y}_{1:k})$, where the state sequence can be modelled as a Markov chain. Leveraging this property, the past information can be effectively summarised by the state at the previous time step Elfring et al. (2021). Consequently, the target PDF can be expressed as:

$$p(\boldsymbol{x}_k|\boldsymbol{y}_{1:k}) = \frac{p(\boldsymbol{y}_k|\boldsymbol{x}_k)p(\boldsymbol{x}_k|\boldsymbol{y}_{1:k-1})}{p(\boldsymbol{y}_k|\boldsymbol{y}_{1:k-1})} \tag{12}$$

Where $p(\boldsymbol{y}_k|\boldsymbol{x}_k)$ represents the conditional probability of measurements given the states. The term $p(\boldsymbol{y}_k|\boldsymbol{y}_{1:k-1})$ denotes the marginal PDF, serving as a normalisation factor dependent solely on measurements. Finally, $p(\boldsymbol{x}_k|\boldsymbol{y}_{1:k-1})$ represents the prior. The procedure of PF algorithm can be divided into the steps as follows:

- **Initialisation**: Sample N particles $\boldsymbol{x}^i_0$ from an initial prior distribution $p(\boldsymbol{x}_0)$ and assign them equal weights:

$$\begin{aligned} &\boldsymbol{x}^i_0 \sim p(\boldsymbol{x}_0) \\ &w^i_0 = 1/N \quad i = 1, ..., N \end{aligned} \tag{13}$$

  The initial prior distribution can be obtained from any other estimators, such as the Least Squares estimator, at the first epoch. the superscript i refers to the i-th particle. It should be noticed that the superscript (i) means the i-th GNSS satellite, which should be distinguished from i.

- **Iterative estimation**: Execute the following steps when new measurements are available.

  1. Predict the position of particles based on the importance distribution:

$$\boldsymbol{x}^i_k \sim p(\boldsymbol{x}_k \mid \boldsymbol{x}_{k-1}) \quad i = 1, ..., N \tag{14}$$

     which exploits the dynamic model of the state-space model Särkkä (2013).

  2. Update weights of particles based on:

$$w^i_k \propto w^i_{k-1} p(\boldsymbol{y}_k \mid \boldsymbol{x}^i_k) \tag{15}$$

     where $p(\boldsymbol{y}_k \mid \boldsymbol{x}^i_k)$ represents the conditional probability distribution of the measurements, known as the measurement likelihood, given the i-th particle, and w^i_{k-1} denotes the weights from the previous epoch. Subsequently, the updated weights $\{w^i_k\}^N_{i=1}$ are normalised to ensure their collective sum equals one.

  3. Compute the effective number of particles Särkkä (2013):

$$N_{ef} = \left(\sum_{i=1}^{N} \left(w^i_k\right)^2\right)^{-1} \tag{16}$$

Then, the effective number of particles, denoted as N_{ef}, is compared with a predefined threshold, N_{th}. If N_{ef} is less than or equal to N_{th}, resampling is carried out, and the weights are reset to $w_k^i = 1/N$. This procedure helps prevent particle degeneracy, a scenario where the majority of weights approach zero Cappé et al. (2007).

3. GNSS multipath/NLoS detection

To ensure the performance under scenarios where satellite visibility is limited, the proposed GNSS multipath/NLoS detection method is based on the PF techniques, which can leverage the consistency from both space and time domains.

a) Pseudorange Innovation

Innovation is a common concept in the Extended Kalman Filter (EKF) framework. This work aims to extend the definition for the PF. The innovation in a PF is the difference between the measurement vector and the nominal measurement vector. The nominal measurement vector is the output of the measurement model given as input the predicted states, which in turn are given by the one-step prediction through the dynamic model given the estimated states of the previous epoch. Based on (6), the nominal measurement for pseudorange $\hat{\rho}_k^{-(i)}$ is written as:

$$\hat{\rho}_k^{-(i)} = \hat{r}_k^{-(i)} + \hat{\delta t}_{u,k}^{-} - \hat{\delta t}_k^{-(i)} + \hat{I}_k^{-(i)} + \hat{T}_k^{-(i)} + \hat{F}_{\rho,k}^{-(i)} \tag{17}$$

where the superscript " $-$ " indicates that the corresponding variable is predicted (a priori). It is worth mentioning that $\hat{F}_{\rho,k}^{-(i)}$ is assumed to be zero to detect GNSS multipath/NLoS. By subtracting (17) from (6), the pseudorange innovation $v_{\rho,k}^{(i)}$ can be written as:

$$\begin{aligned} v_{\rho,k}^{(i)} &= \rho_k^{(i)} - \hat{\rho}_k^{-(i)} \\ &= (r_k^{(i)} - \hat{r}_k^{-(i)}) + (\delta t_{u,k} - \hat{\delta t}_{u,k}^{-}) - (\delta t_k^{(i)} - \hat{\delta t}_k^{-(i)}) + \\ &(I_k^{(i)} - \hat{I}_k^{-(i)}) + (T_k^{(i)} - \hat{T}_k^{-(i)}) + (F_{\rho,k}^{(i)} - \hat{F}_{\rho,k}^{-(i)}) + \epsilon_{\rho,k}^{(i)} \\ &= \Delta r_k^{(i)} + \Delta\delta t_{u,k} - \Delta\delta t_k^{(i)} + \Delta I_k^{(i)} + \Delta T_k^{(i)} + \Delta F_{\rho,k}^{(i)} + \epsilon_{\rho,k}^{(i)} \end{aligned} \tag{18}$$

The innovation for each satellite incorporates information from both the previous epoch (nominal measurement) and the current epoch (real measurement), enabling the assessment of consistency in the space domain. Similarly, examining multiple innovations from different satellites at the same epoch allows for the evaluation of consistency in the time domain.

b) Pseudorange Innovation threshold

Referring to (18), the pseudorange innovation value encompasses all terms except $\Delta F_{\rho,k}^{(i)}$ under multipath/NLoS-free conditions. Thus, the accuracy of the state-space model and the estimation precision from the previous epoch dictate the innovation value. In the absence of multipath/NLoS and when the filtering solution approximates the true solution adequately, the innovation remains bounded, a point that will be empirically validated in the experimentation section. However, the occurrence of a multipath/NLoS can significantly alter pseudorange measurements, consequently impacting the innovation. For instance, multipath-induced faults can lead to deviations up to $70\,\mathrm{m}$ for GPS L1 C/A signals Braasch (1996). Hence, it becomes crucial to monitor innovation values to detect GNSS multipath/NLoS, typically by setting a threshold $v_{\rho,k,th}^{(i)}$ on the innovation.

c) Advantages of PF

This subsection will discuss two advantages of using the PF-based techniques in detail to provide a theoretical basis for the PF-based multipath/NLoS mitigation method. The EKF, which has been adopted by some research Zhu et al. (2018a); Joerger and Pervan (2013), is selected as a reference for comparison. In some cases, the measurement biases caused by multipath/NLoS are small, and their contribution to the innovation can be overwhelmed by the dynamics of the user, atmosphere model error, and other terms. As a consequence, some small-value multipath/NLoS can cause missed detections. PF can guarantee stronger constraints to divergence in such cases. The estimated states in PF are computed as a weighted average of the particles. Therefore, an estimate can not be outside the support of where the probability density is samples at. The range of values of these particles is driven by the process noise and hence by the dynamics of the user. The meter-level range between particles in land vehicle applications can protect the filter from diverging quickly in case of missed detections. However, the EKF behaves differently. Considering the presence of multipath/NLoS $\boldsymbol{F}_{\rho,k}$ in a set of input measurements, the update step can be expanded as follows:

$$\hat{\boldsymbol{x}}_k = \hat{\boldsymbol{x}}_k^{-} + \boldsymbol{K}_k(\boldsymbol{y}_k + \boldsymbol{F}_{\rho,k} - \boldsymbol{H}_k\hat{\boldsymbol{x}}_k^{-}) \tag{19}$$

where $\boldsymbol{K}_k$ is the Kalman gain. Hence, the estimated error due to the multipath/NLoS $\Delta\hat{\boldsymbol{x}}_k$ can be written as:

$$\Delta\hat{\boldsymbol{x}}_k = \boldsymbol{K}_k \boldsymbol{F}_{\rho,k} \tag{20}$$

which can be of several meters, thus resulting in loose constraints to states compared to the PF. The second advantage is that the PF can utilise non-Gaussian and possibly multi-modal noise models, which may be more suitable to model the error statistics of measurements affected by multipath/NLoS and protect from false alarms which may arise in harsh conditions. This can increase the robustness against false alarms and thus motivates the design of this work.

4. PF measurement function

The typical pseudorange measurement model assumes the multipath/NLoS term is zero, so it might become biased when such events indeed occur. As a result, the unmodelled multipath/NLoS can produce large errors in the estimated states. To mitigate their effect, this work aims at modeling multipath/NLoS in the measurement function by estimating the $F_{\rho,k}^{(i)}$ term. To be specific, when the innovation is larger than a threshold, it is assumed that its value is mostly driven by the multipath/NLoS term, so $\hat{F}_{\rho,k}^{(i)}$ is estimated as the value of the innovation:

$$\hat{F}_{\rho,k}^{(i)} := \begin{cases} v_{\rho,k}^{(i)} & \text{for } v_{\rho,k}^{(i)} \geq v_{\rho,k,th}^{(i)} \\ 0 & \text{for } v_{\rho,k}^{(i)} < v_{\rho,k,th}^{(i)} \end{cases} \tag{21}$$

Substituting $\hat{F}_{\rho,k}^{(i)}$ into (6), a modified measurement model is obtained which accounts for multipath/NLoS. This design is graphically shown in Fig. 1a, which compares the original likelihood function without multipath/NLoS compensation and the multipath/NLoS-compensated likelihood function. The unnormalised particle weights obtained from the original likelihood function can be represented as:

$$w_k^i = w_{k-1}^i p(\boldsymbol{y}_k \mid \hat{\boldsymbol{x}}_k^{-,i}, \boldsymbol{F}_{\rho,k}^{(i)} = \boldsymbol{0}) = w_{k-1}^i \prod_{m=1}^{M} w_{k,m}^i \tag{22}$$

While the unnormalised particle weights obtained from the multipath/NLoS-compensated likelihood function can be computed as:

$$\tilde{w}_k^i = w_{k-1}^i p(\boldsymbol{y}_k \mid \hat{\boldsymbol{x}}_k^{-,i}, \boldsymbol{F}_{\rho,k}^{(i)} = \hat{\boldsymbol{F}}_{\rho,k}^{(i)}) = w_{k-1}^i \prod_{m=1}^{M} \tilde{w}_{k,m}^i \tag{23}$$

To enhance the robustness of the proposed mitigation method, this work leverages the concept of Soft Information introduced in Conti et al. (2019). This involves combining the original likelihood function with the likelihood associated with the multipath/NLoS term. By integrating these two sources of information, the method can effectively account for false alarms and improve overall multipath/NLoS detection accuracy. This work proposes an adaptive way to combine these two likelihoods together to obtain a new non-Gaussian likelihood function determining the weight of each particle. Fig. 1b depicts this adaptive combination design. The multipath/NLoS detection and bias estimation are more reliable when only one or two satellites are affected. In such cases, correcting the measurements proves to be the most effective strategy. Conversely, when multiple measurements are detected to be impacted by multipath/NLoS at the same epoch, the reliability of $\hat{F}_{\rho,k}^{(i)}$ decreases. Therefore, the confidence level of the likelihood $p(\boldsymbol{y}_k \mid \hat{\boldsymbol{x}}_k^{-,i}, \boldsymbol{F}_{\rho,k}^{(i)})$ should be decreased. As a result, the unnormalised combined particle weights $w_{adp,k}^i$ are the sum of w_k^j and $\tilde{w}_k^j$ with adaptive weights:

$$w_{adp,k}^i = h_1 \cdot w_k^j + h_2 \cdot \tilde{w}_k^j \tag{24}$$

where the weights h_1 and h_2 can be computed according to the following adaptive strategy:

$$\begin{aligned} h_1 &= \frac{\text{number of detected multipath/NLoS satellites}}{\text{number of visible satellites}} \\ h_2 &= 1 - h_1 \end{aligned} \tag{25}$$

5. Divergence protection

The effectiveness of the proposed PF-based method relies on the assumption that the navigation solution from the previous epoch maintains acceptable accuracy. If the filter produces a solution with significant errors, it becomes challenging to estimate

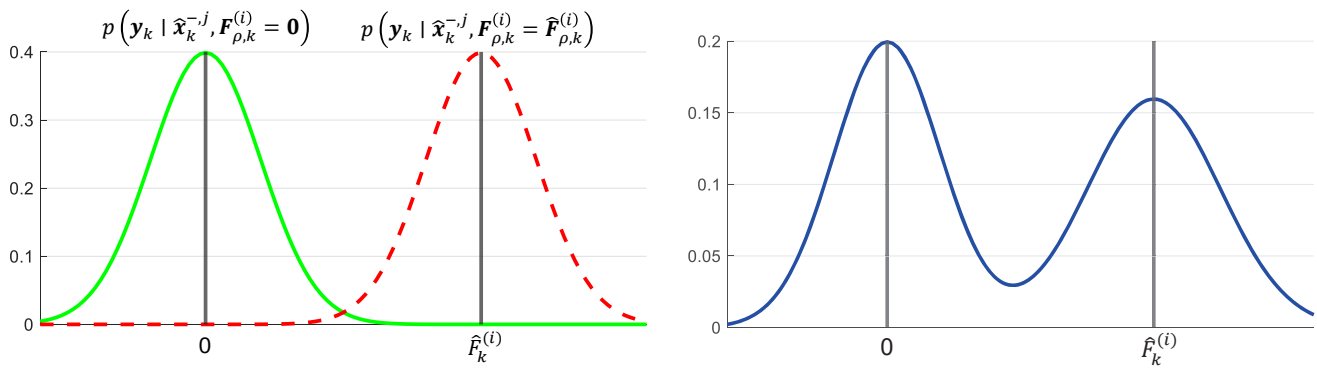

(a) Modification of the likelihood function

(b) Adaptive PF strategy

Figure 1: Comparison of proposed likelihood function for the PF. (a) A comparison between the multipath/NLoS-compensated (red) and the legacy likelihood function (green); (b) Combination the multipath/NLoS-compensation and the legacy likelihood functions.

reliable innovation values. Consequently, in some instances it can be useful to re-initialise the filter to avoid this problem. A Generalized Least Square (GLS) estimator with classical RAIM-Fault Detection and Exclusion (FDE) is employed to monitor the divergence in filtering solutions. The current navigation solution is considered invalid and needs to be re-initialised under the following two conditions:

- The distance between positions obtained by the filter and by the GLS estimator with RAIM-FDE is larger than $50\,\mathrm{m}$ while the visible satellite number is larger than 12.
- The receiver has lost lock on all satellites for more than a second.

III. EXPERIMENT AND RESULTS

1. Experimental settings

This experiment leverages a real-world open-source dataset UrbanNav Hsu et al. (2021), provided by Hong Kong Polytechnic University, to verify the effectiveness of the proposed method. The dataset was collected in Shinjuku, Tokyo, in harsh GNSS scenario with multipath and NLoS. This research utilises $10\,\mathrm{Hz}$ of PVT step size and signals from four constellations, including GPS L1 C/A, GLONASS G1 C/A, Galileo E1, and BeiDou B1I. State estimation errors are computed w.r.t. a reference trajectory obtained with an Real Time Kinematic (RTK)/INS integration system. Figure 2a depicts the whole trajectory of the dataset. The sky plot with Carrier-to-Noise Density Ratio C/N_0 is shown in Figure 2b. As can be seen, many satellites have low C/N_0, which might indicate the presence of multipath and NLoS. The position, velocity, and clock bias of satellites are computed from the broadcast ephemeris, as could be done by real-time applications. Tropospheric delay is estimated using Saastamoinen model, while ionospheric delay is estimated from one-day ahead predicted Global Ionospheric Maps (GIM) from Center for Orbit Determination in Europe (CODE). The inter-system clock biases are calculated based on the model parameters provided by International GNSS Service (IGS). The particle number of the PF is fixed as 1000 and the resampling threshold is set to 0.1. It is assumed that the measurement errors are Gaussian, with zero means and known covariances. These covariances are computed based on an elevation-based model whose coefficients are shown in Table. 1. Table 2 recaps the settings for process noise covariance. The value of the threshold on the pseudorange innovation $v_{\rho,k,th}^{(i)}$ is determined by empirical attempts and is set as $5\,\mathrm{m}$. This experiment first implemented the proposed PF-based method, which is named PF-ADP in the following discussion.

Table 1: Measurement noise coefficients for pseudorange and pseudorange rate.

Pseudorange		Pseudorange rate	
a_ρ	b_ρ	$a_{\dot{\rho}}$	$b_{\dot{\rho}}$
$0.5\,\mathrm{m}$	$0.3\,\mathrm{m}$	$0.05\,\mathrm{m/s}$	$0.03\,\mathrm{m/s}$

To validate the performance of the proposed method, this research also implements two classical methods as references. The first is the classical RAIM-FDE, as described in Zhu et al. (2018b). In this method, the fault exclusion assumes that at most one satellite is faulty. If the chi-squared test cannot be satisfied after testing all fault subsets, the navigation solution is marked

(a) Vehicle trajectory in the Shinjuku dataset.

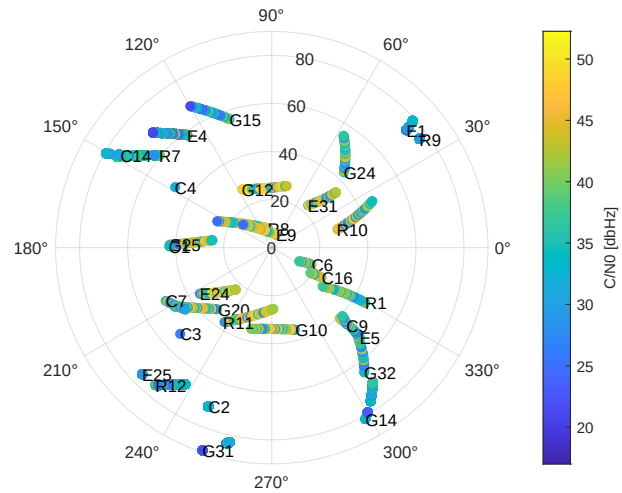

(b) Sky plot with signal strength C/N_0

Figure 2: Experimental scenarios.

Table 2: Process noise parameters.

$a_{max,X}$	$a_{max,Y}$	$a_{max,Z}$	$\delta a_{max,u}$
$2.5\,\mathrm{m/s^2}$	$2.5\,\mathrm{m/s^2}$	$2.5\,\mathrm{m/s^2}$	$0.4\,\mathrm{m/s^3}$

as invalid. Secondly, following the approach proposed in Zhu et al. (2018a), this research implements an EKF-FDE method, utilising the same parameter settings as the PF-ADP method.

2. Estimation accuracy

Experimental results present a comprehensive comparison between the proposed method and two classical methods. Figure. 3 illustrates the Cumulative Distribution Function (CDF)s of horizontal and vertical positioning errors, while Table. 3 provides positioning errors at different percentiles within these CDFs. Notably, the proposed PF-ADP method not only ensures high accuracy compared to classical methods but also effectively prevents the occurrence of large errors induced by multipath and NLoS effects. Table. 4 summarises the 3D Root Mean Squared Error (RMSE) and mean positioning errors for all implemented methods in this experiment. In the case of PF-ADP, CDF and RMSE results are averaged across 20 runs. Table 4 also presents the availability of navigation solutions, defined as the ratio between navigation solutions obtained by each estimator and the total number of epochs. In the case of RAIM-FDE, if the measurement redundancy is insufficient or one fault assumption fails, the navigation solution is marked as unavailable. For EKF-FDE and PF-ADP, if all signals lose lock for more than $1\,\mathrm{s}$ and the initialisation of the filter fails, no solution is available. The results demonstrate that filtering methods offer higher availability compared to traditional RAIM-FDE in challenging GNSS conditions.

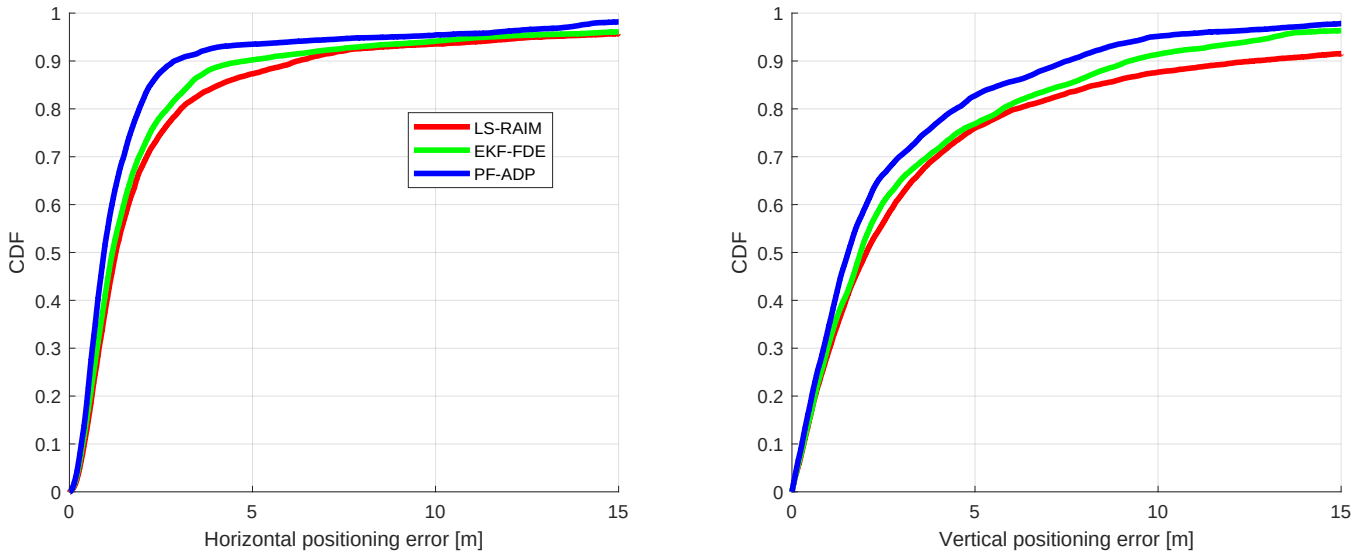

Figure 3: CDFs horizontal (left) and vertical (right) positioning errors for different multipath/NLoS mitigation methods.

Table 3: Horizontal and vertical positioning errors at different percentiles of CDFs.

	Horizontal [m]				Vertical [m]			
	50th	75th	90th	99th	50th	75th	90th	99th
RAIM-FDE	1.2668	2.5095	12.6849	44.4291	2.0359	4.7982	25.0405	63.1595
EKF-FDE	1.1741	2.2022	11.4075	26.7038	1.8744	4.5163	13.1415	52.2684
PF-ADP	0.9453	1.6702	8.7259	17.8284	1.5323	3.6384	9.7879	45.1657

Table 4: 3D RMSEs and mean errors for different multipath/NLoS mitigation methods.

	RMSE [m]	Mean error [m]	Availability
RAIM-FDE	15.6818	6.9351	70.00%
EKF-FDE	11.3112	5.5782	99.02%
PF-ADP	7.6907	4.0647	99.02%

Figure. 4 depicts the time series of positioning errors under the East-North-Up (ENU) frame, in the case of PF-ADP from a single run of the Monte Carlo experiment. Additionally, the bottom plot presents the number of faulty satellites due to multipath/NLoS, as detected by the threshold in the PD-ADP. The overall trajectories obtained from three different methods are shown in Figure. 5.

3. Discussion

Based on the experimental results obtained from a single run of the PF-ADP method, Figure. 6 illustrates the pseudorange innovations from the PF and the corresponding threshold to detect the occurrence of multipath/NLoS. Additionally, Figure. 7 presents the percentage of epochs during which multipath/NLoS is detected.

IV. CONCLUSION

This research introduced a PF-based method for mitigating multipath/NLoS effects in GNSS. Firstly, the definition of innovation is extended to the PF framework, enabling the detection of multipath/NLoS. Subsequently, an adaptive strategy is designed to generate a multi-modal likelihood function, reducing the impact of multipath/NLoS. The effectiveness of the proposed method is validated using an open-source dataset collected in a challenging scenario. The proposed method achieves an accuracy of

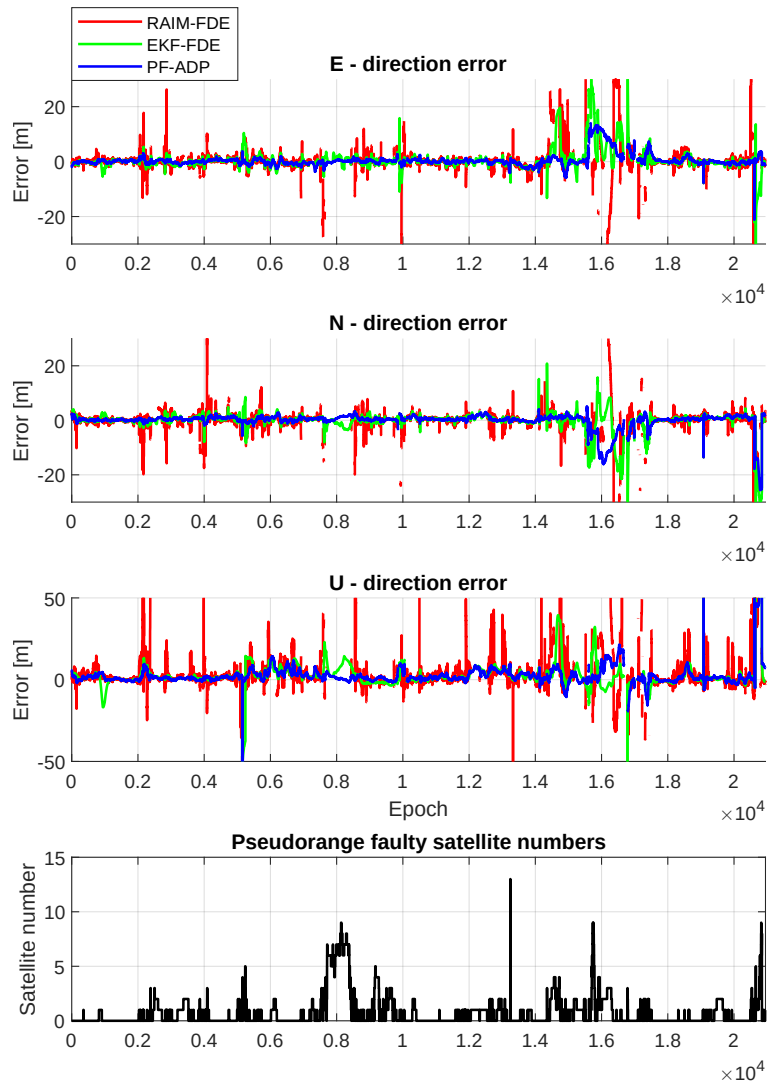

Figure 4: Time series of positioning errors for East, North, and Up directions. The bottom plot provides the time series of faulty satellite numbers with multipath/NLoS detected by the PD-ADP method.

$7.6907\,\mathrm{m}$ in terms of RMSE. This outperforms two baseline methods: RAIM-FDE with an RMSE of $15.6818\,\mathrm{m}$ and EKF-FDE with an RMSE of $11.3112\,\mathrm{m}$. Future work is going to focus on other strategies for combining likelihoods under different hypothesis, as well as setting the value of the threshold adaptively.

ACKNOWLEDGEMENTS

Y. Guo acknowledges the Chinese Scholarship Council (CSC). All authors acknowledge the research teams from Tokyo University of Marine Science and Technology (Japan) and Hong Kong Polytechnic University (Hong Kong) for collecting and sharing the dataset.

ABBREVIATIONS

The following abbreviations are used in this paper:

CDF Cumulative Distribution Function

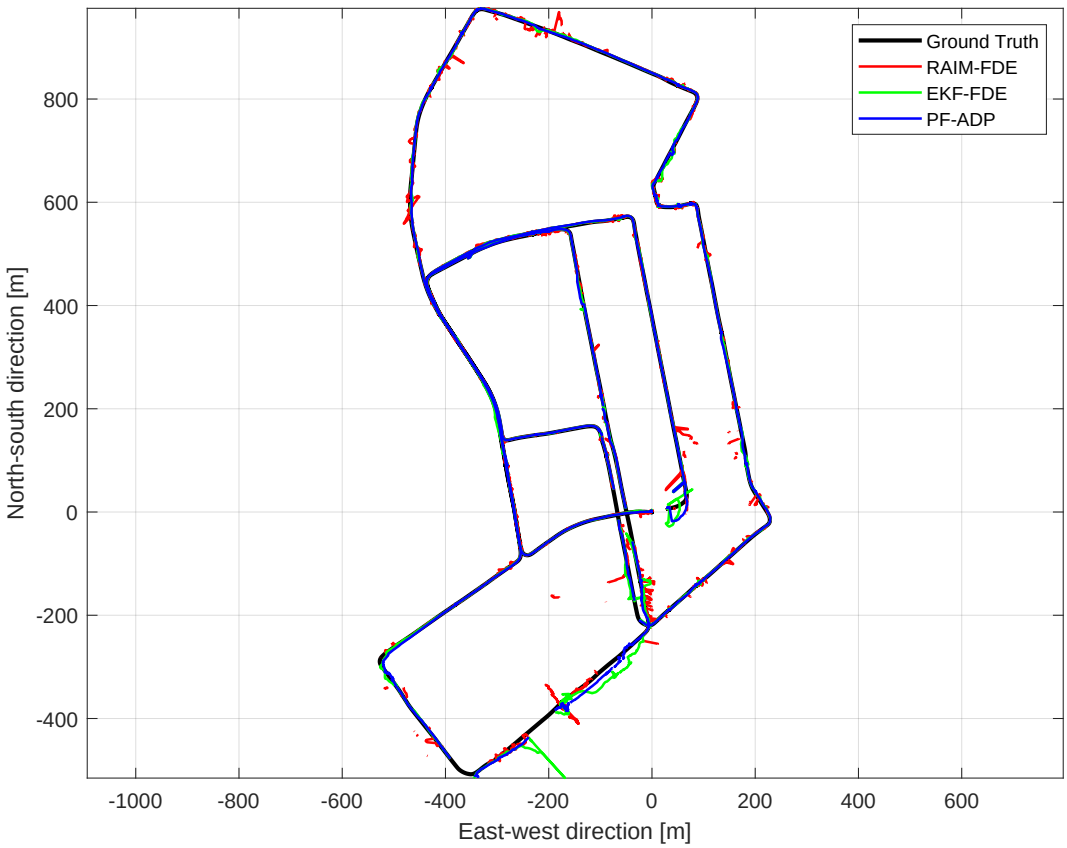

Figure 5: Positioning trajectories obtained by three different multipath/NLoS mitigation methods with respect to the ground truth.

CODE Center for Orbit Determination in Europe
EKF Extended Kalman Filter
ENU East-North-Up
FDE Fault Detection and Exclusion
GIM Global Ionospheric Maps
GLS Generalized Least Square
GNSS Global Navigation Satellite System
IGS International GNSS Service
INS Inertial Navigation System
NLoS Non-Line-of-Sight
PDF Probability Density Function
PF Particle Filter
PVT Position, Velocity and Time
RAIM Receiver Autonomous Integrity Monitoring
RMSE Root Mean Squared Error
RTK Real Time Kinematic

REFERENCES

Blanch, J., Walter, T., Enge, P., Lee, Y., Pervan, B., Rippl, M., and Spletter, A. (2012). Advanced RAIM user algorithm description: Integrity support message processing, fault detection, exclusion, and protection level calculation. In *Proceedings of the 25th International Technical Meeting of The Satellite Division of the Institute of Navigation (ION GNSS 2012)*, pages 2828–2849.

Braasch, M. S. (1996). GPS multipath model validation. In *Proceedings of Position, Location and Navigation Symposium-PLANS'96*, pages 672–678. IEEE.

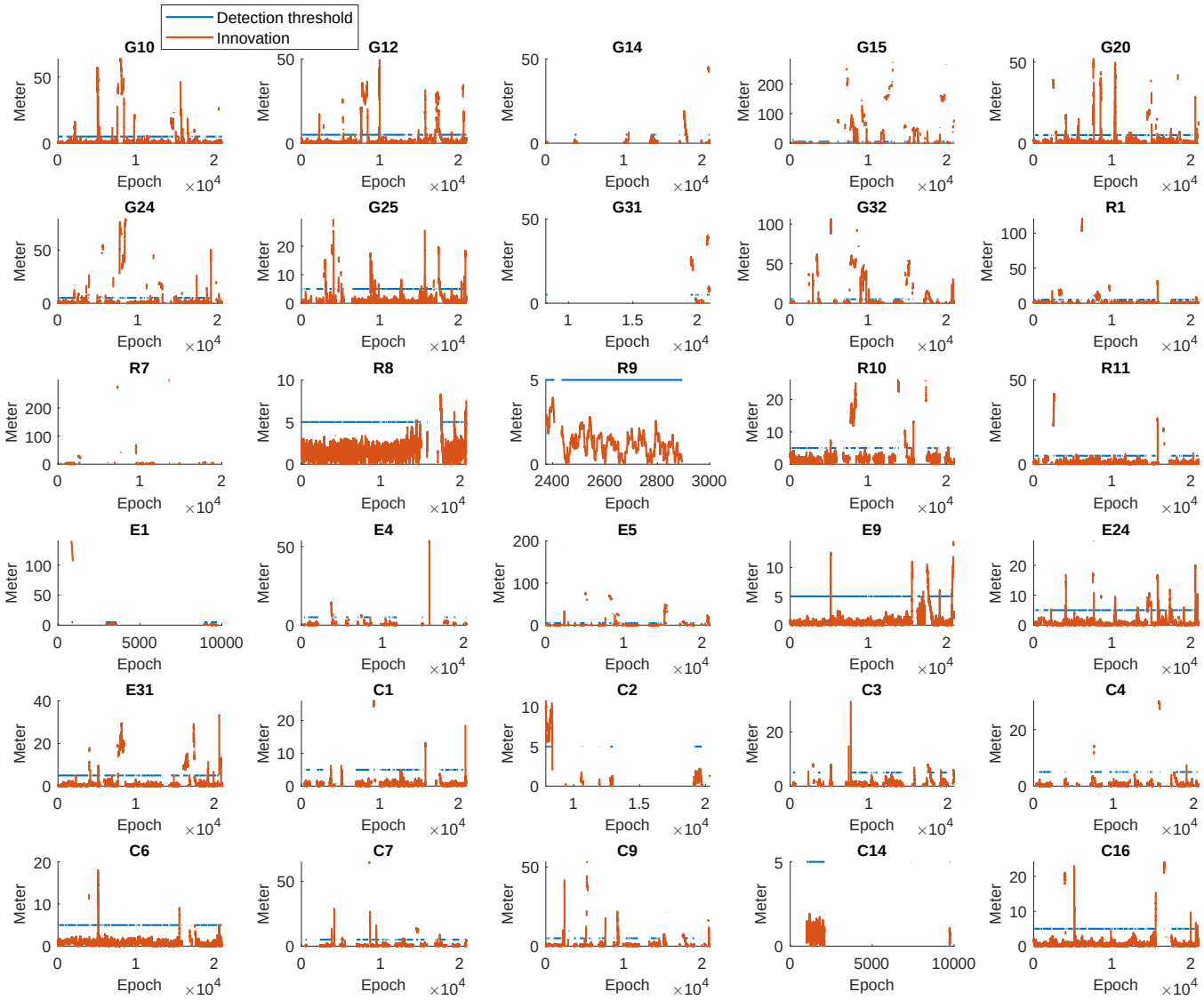

Figure 6: The multipath/NLoS detection thresholds and the innovations for pseudorange measurements in the PF-ADP method.

Cappé, O., Godsill, S. J., and Moulines, E. (2007). An overview of existing methods and recent advances in sequential monte carlo. *Proceedings of the IEEE*, 95(5):899–924.

Chang, J., Zhan, X., Zhai, Y., Wang, S., Lin, K., and Yang, R. (2022). Vector angle grouping-based solution separation for multipath/NLOS detection and exclusion with the enhancement of doppler test. *GPS Solutions*, 26(4):121.

Chen, X., Dovis, F., Peng, S., and Morton, Y. (2013). Comparative studies of GPS multipath mitigation methods performance. *IEEE Transactions on Aerospace and Electronic Systems*, 49(3):1555–1568.

Conti, A., Mazuelas, S., Bartoletti, S., Lindsey, W. C., and Win, M. Z. (2019). Soft information for localization-of-things. *Proceedings of the IEEE*, 107(11):2240–2264.

Elfring, J., Torta, E., and van de Molengraft, R. (2021). Particle filters: A Hands-On Tutorial. *Sensors*, 21(2).

EUSPA (2022). EUSPA EO and GNSS Market Report. Technical report.

Groves, P. D. and Jiang, Z. (2013). Height aiding, C/N0 weighting and consistency checking for GNSS NLOS and multipath mitigation in urban areas. *The Journal of Navigation*, 66(5):653–669.

Groves, P. D., Jiang, Z., Skelton, B., Cross, P. A., Lau, L., Adane, Y., and Kale, I. (2010). Novel multipath mitigation methods

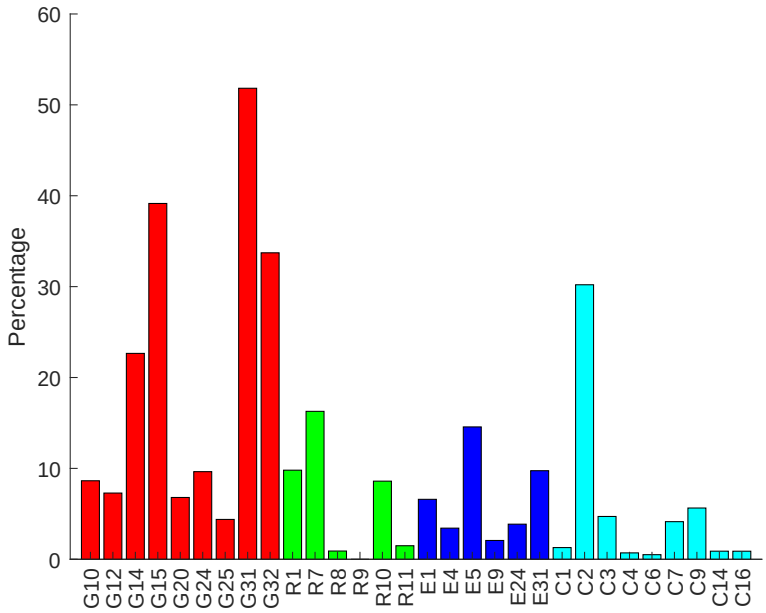

Figure 7: The percentage of PF-ADP innovations exceeding the thresholds for multipath/NLoS detection varies among different satellites.

using a dual-polarization antenna. In *Proceedings of the 23rd International Technical Meeting of The Satellite Division of the Institute of Navigation (ION GNSS 2010)*, pages 140–151.

Gupta, S. and Gao, G. X. (2019). Particle raim for integrity monitoring. In *Proceedings of the 32nd International Technical Meeting of the Satellite Division of The Institute of Navigation (ION GNSS+ 2019)*, pages 811–826.

Hsu, L.-T. (2017). GNSS multipath detection using a machine learning approach. In *2017 IEEE 20th International Conference on Intelligent Transportation Systems (ITSC)*, pages 1–6. IEEE.

Hsu, L.-T., Kubo, N., Wen, W., Chen, W., Liu, Z., Suzuki, T., and Meguro, J. (2021). Urbannav: An open-sourced multisensory dataset for benchmarking positioning algorithms designed for urban areas. In *Proceedings of the 34th International Technical Meeting of the Satellite Division of The Institute of Navigation (ION GNSS+ 2021)*, pages 226–256.

Joerger, M. and Pervan, B. (2013). Kalman filter-based integrity monitoring against sensor faults. *Journal of Guidance, Control, and Dynamics*, 36(2):349–361.

Joerger, M. and Pervan, B. (2016). Fault detection and exclusion using solution separation and chi-squared ARAIM. *IEEE Transactions on Aerospace and electronic systems*, 52(2):726–742.

McGraw, G. A. and Braasch, M. S. (1999). GNSS multipath mitigation using gated and high resolution correlator concepts. In *Proceedings of the 1999 national technical meeting of the institute of navigation*, pages 333–342.

McGraw, G. A., Groves, P. D., and Ashman, B. W. (2020). Robust positioning in the presence of multipath and NLOS GNSS signals. *Position, navigation, and timing technologies in the 21st century: integrated satellite navigation, sensor systems, and civil applications*, 1:551–589.

Medina, D., Gibson, K., Ziebold, R., and Closas, P. (2018). Determination of pseudorange error models and multipath characterization under signal-degraded scenarios. In *Proceedings of the 31st International Technical Meeting of the Satellite Division of the Institute of Navigation, ION GNSS+ 2018*.

Mohanty, A., Gupta, S., and Gao, G. X. (2021). A particle-filtering framework for integrity risk of gnss-camera sensor fusion. *Navigation*, 68(4):709–726.

Särkkä, S. (2013). *Bayesian filtering and smoothing*. Number 3. Cambridge university press.

Spilker Jr, J. J., Axelrad, P., Parkinson, B. W., and Enge, P. (1996). *Global Positioning System: theory and applications, volume I*. American Institute of Aeronautics and Astronautics.

Strode, P. R. and Groves, P. D. (2016). GNSS multipath detection using three-frequency signal-to-noise measurements. *GPS solutions*, 20:399–412.

Sun, Y., Yao, Z., and Lu, M. (2022). Extended Double-Delta Correlator Technique for GNSS Multipath Mitigation. *IEEE Transactions on Aerospace and Electronic Systems*, 59(2):1758–1773.

Taghdisi, E., Ghaffarian, M. S., and Mirzavand, R. (2021). Low-profile substrate integrated choke rings for GNSS multipath mitigation. *IEEE Transactions on Antennas and Propagation*, 70(3):1706–1718.

Vagle, N., Broumandan, A., Jafarnia-Jahromi, A., and Lachapelle, G. (2016). Performance analysis of GNSS multipath mitigation using antenna arrays. *The Journal of Global Positioning Systems*, 14(1):1–15.

Vilà-Valls, J., Linty, N., Closas, P., Dovis, F., and Curran, J. T. (2020). Survey on signal processing for GNSS under ionospheric scintillation: Detection, monitoring, and mitigation. *NAVIGATION: Journal of the Institute of Navigation*, 67(3):511–535.

Wang, J., Stewart, M. P., and Tsakiri, M. (1998). Stochastic modeling for static GPS baseline data processing. *Journal of Surveying Engineering*, 124(4):171–181.

Wang, S., Zhan, X., Zhai, Y., and Liu, B. (2020). Fault detection and exclusion for tightly coupled GNSS/INS system considering fault in state prediction. *Sensors*, 20(3):590.

Wang, Y. and Huang, Z. (2020). MEDLL on-strobe correlator: a combined anti-multipath technique for GNSS signal tracking. *The Journal of Navigation*, 73(3):658–677.

Xu, B., Jia, Q., and Hsu, L.-T. (2019). Vector tracking loop-based GNSS NLOS detection and correction: Algorithm design and performance analysis. *IEEE transactions on instrumentation and measurement*, 69(7):4604–4619.

Zhu, N., Betaille, D., Marais, J., and Berbineau, M. (2018a). Extended Kalman filter (EKF) innovation-based integrity monitoring scheme with C/N 0 weighting. In *2018 IEEE 4th International Forum on Research and Technology for Society and Industry (RTSI)*, pages 1–6. IEEE.

Zhu, N., Marais, J., Bétaille, D., and Berbineau, M. (2018b). GNSS position integrity in urban environments: A review of literature. *IEEE Transactions on Intelligent Transportation Systems*, 19(9):2762–2778.